Ocean Science

Eddy characteristics in the northern South China Sea as inferred from Lagrangian drifter data

Jiaxun Li[1,2], Ren Zhang[1], and Baogang Jin[3]

[1]Key Laboratory of Ocean Hydrology Environment, Institute of Meteorology, PLA University of Science and Technology, Nanjing, China
[2]State Key Laboratory of Satellite Ocean Environment Dynamics, Second Institute of Oceanography, SOA, Hangzhou, China
[3]Beijing Applied Institute of Meteorology, Beijing, China

Abstract. Cyclonic and anticyclonic eddies from large scale to submesoscale in the northern South China Sea (NSCS) have been statistically characterized based on the satellite-tracked Lagrangian drifters using our developed geometric eddy identification method. There are in total 2208 eddies identified, 70 % of which are anticyclonic eddies. If the submesoscale eddies are eliminated, the other eddies in the NSCS will show a 1.2:1 ratio of the number of anticyclones (210) to the number of cyclones (171). The spatial distribution of the eddies is regional: in southwest of Taiwan, the number of anticyclones dominates the number of cyclones, and most of them are the submesoscale anticyclones with small radii; in contrast, the large and medium cyclonic eddies are a little more than the same scale anticyclonic eddies in northwest of Luzon. The temporal distribution of eddy number in the NSCS has a close relation with the Asian monsoon. The number of the large and medium eddies peaks during the winter monsoon, while the submesoscale eddies are apt to generate in the summer monsoon. The spatial and temporal patterns have a good agreement with the results of the sea surface height anomaly (SSHA). The maximum and mean tangential velocities of anticyclones (cyclones) are 40 (30) cm s^{-1} and 25 (15) cm s^{-1}, respectively. The calculated normalized vorticities from drifters suggest that although the mesoscale eddies may be considered in geostrophic balance, ageostrophic dynamics and centrifugal effects may play an important role for the growth and decay of the mesoscale cores.

1 Introduction

The South China Sea (SCS) is the largest semi-closed marginal sea in the western Pacific Ocean, connecting in the north with the Pacific through the deep Luzon Strait (depth > 2000 m) and with the East China Sea through the shallow Taiwan Strait (depth < 200 m), and in the south with the Sulu and Java Seas through a number of shallow passages (Fig. 1). The surface area of the SCS is about 3.5 million square kilometers, with the mean depth of 1800 m and the maximum depth of 5400 m.

The patterns of the whole SCS upper circulation are related to the Asia monsoon, with significant impact of Kuroshio on the northern part of circulation through Luzon Strait (Qu, 2000). In winter, the general circulation in the SCS is a cyclonic gyre, while in summer, there is a cyclonic gyre north of 12° N and an anticyclonic gyre south of it (Su, 2004). Embedded in the large gyres are many energetic mesoscale eddies observed by both hydrographic (e.g. Chu et al., 1998; Su et al., 1999) and satellite altimeter data (e.g. Shaw et al., 1999; Hwang and Chen, 2000; Wang et al., 2003, 2006).

The NSCS lies north of 16° N and is bordered by the China Mainland, Vietnam, Taiwan Island, Luzon Island and Hainan Island (Fig. 2a), and is connected with the Philippine Sea and the East China Sea via Luzon Strait and Taiwan Strait, respectively. Eddies in the NSCS have received much attention in the past decades. Eddy shedding into the NSCS from Kuroshio meander was studied by many work (e.g. Li et al., 1998; Jia and Liu, 2004; Yuan et al., 2006). Based on the satellite data, Yuan et al. (2007) depicted the generation and propagation of the anticyclonic eddies northwest of Luzon Island. Chow et al. (2008) studied the variations and characteristics of a mesoscale cyclonic eddy in southwest of the Dongsha Islands identified by a composite of drifters, satellite altimeter data, AVHRR and SeaWIFS images. In order to

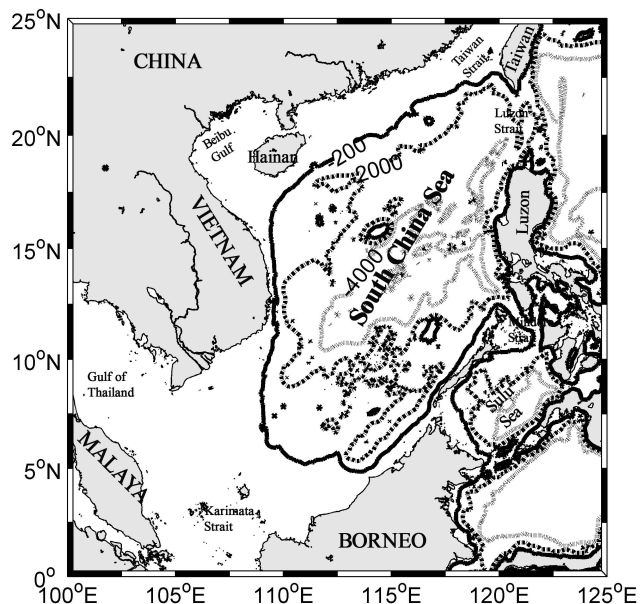*Correspondence to:* Jiaxun Li
(lijiaxun2009@yahoo.com.cn)

Fig. 1. Bathymetry of the SCS, with only −200 m, −2000 m, and −4000 m contours plotted.

Fig. 2. (a) All the 576 drifter trajectories in the NSCS from 1979 to 2010 in the study region (105° E–122° E, 16° N–25° N). Isobaths are in meter. H: Hainan Island. T: Taiwan Island. L: Luzon Island. **(b)** Number of drifter observations in bins with 0.25° × 0.25°.

understand the vertical structures of eddies and their impact on the upper ocean, the spatial and temporal evolutions of eddies in the NSCS were examined by combining the satellite data with in situ hydrographic data (Wang et al., 2005; D. Wang et al., 2008; Nan et al., 2011).

Despite the fact that the mesoscale eddies in the NSCS have received much attention in the past, studies on the eddy statistic characteristics based on the satellite-tracked drifters are rare, which are a reliable source of in-situ continuous data comparing with satellite remote sensing data and have been extensively utilized in the Bay of Biscay (van Aken, 2002), the eastern South Pacific (Chaigneau and Pizarro, 2005), the Gulf of Mexico slope (Hamilton, 2007), etc. In this study, we will focus on the eddy characteristics in the NSCS with drifters: how do their rotation periods depend on their radii? Can the cyclonic eddies and anticyclonic eddies exhibit distinct characteristics? Do the intraseasonal variations of the eddies in the NSCS directly associate with the Asian monsoon?

The paper is organized as follows. Drifter data is introduced in Sect. 2. Eddy characteristics and eddy statistics in the NSCS are described in Sect. 3. Finally, the paper concludes with a discussion in Sect. 4.

2 Data

The surface satellite – tracked drifter dataset spans from 1979 to the present and is part of the Global Drifter Program/Surface Velocity Program. The drifter has a spherical surface buoy and a semirigid drogue centered at 15 m depth
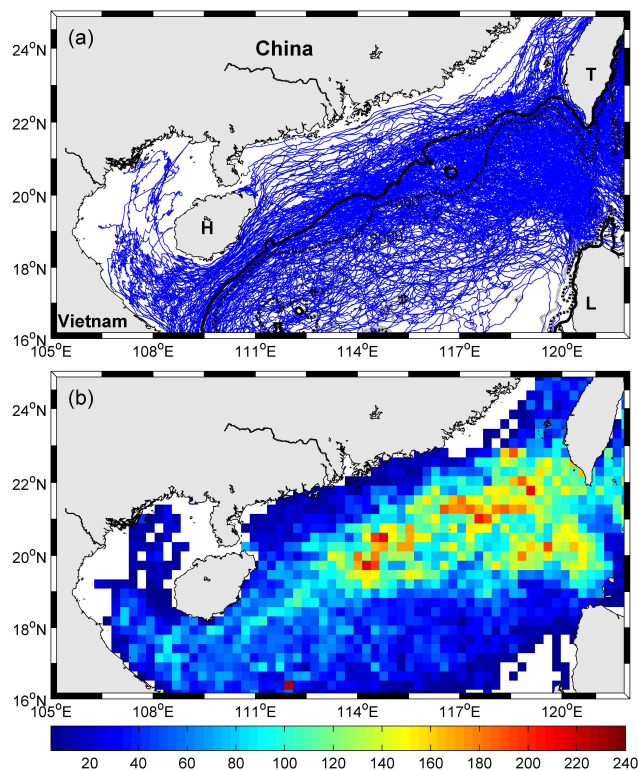
that maintains its shape in high-shear flows. Once deployed, a modern drifter lives an average of around 400 days before ceasing transmission. Occasionally, drifters are picked up by fishermen or lose their drogue and run aground. The Atlantic Oceanographic and Meteorological Laboratory (AOML) received the drifter positions from Doppler shift measurements from Service Argos. AOML's Drifter Data Assembly Center (DAC) assembles these raw drifter locations, applies quality control procedures, and interpolates them to regular 1/4-day intervals using an optimal interpolation procedure known as kriging (Hansen and Poulain, 1996). To remove high-frequency tidal and inertial wave energy and to avoid aliasing the energy into the low-frequency motions, these drifter data were daily averaged (Swenson and Niiler, 1996). The maximum amount of data was observed during the 1990s, corresponding to the World Ocean Circulation Experiment (WOCE) period. In our study area, a total of 576 different drifters, able to exit and return to the area later (considered distinctly), were followed. All the drifter trajectories in the area are shown in Fig. 2a and the spatial distribution of number of drifter observations is shown in Fig. 2b. The number of drifter observations in the center of the study region is very big, whereas the regions near the coast of China and northwest of Luzon Island are poorly sampled. The seasonal

variation of mixed layer depth (MLD) is predominantly an-
nual in the NSCS, where the MLD is deeper than 70 m in
winter and falling below 20 m in summer near the continental
slope south of China. Wind stirring and cooling convection
seem to be dominant in the annual variation in the NSCS,
while the effect of Ekman pumping is not negligible in sum-
mer when both wind stirring and cooling convection become
weak (Qu et al., 2007). Thus it is imperative that the 15 m
drogue depth of drifters be well within the mixed layer in
both seasons.

3 Eddy characteristics and statistics in the NSCS

3.1 Mean flow

The Eulerian mean flow of NSCS was derived by spatially
averaging the current components from the drifters in bins
with $0.25° \times 0.25°$ (Fig. 3). The general pattern of mean
flow is a basin-scale cyclonic gyre, and there is an anticy-
clonic loop pattern within the Luzon Strait, indicating the
Kuroshio occasionally makes a loop in this deep gap of west-
ern boundary (Shaw et al., 1999; Qu, 2000). Furthermore,
a cyclonic eddy (Luzon cold eddy hereafter) often appears
here in winter, which may be excited by the wind stress curl
in offshore of Luzon (Qu, 2000). The obvious mean current
at about 117° E and 18° N is the northern part of the cyclonic
Luzon cold eddy located off the northwest Luzon, which is
controlled by both the local Ekman pumping and remotely
forced basin-scale circulation (Qu, 2000).

3.2 Number and radii of eddies

Statistical analysis of the eddies in the study area is per-
formed using our developed eddy identification method from
drifters. Our method is different from the geometric method
of Boebel et al. (2003), which uses the curvature of drifter
trajectory to identify loops. Our method is based on the def-
inition of a loop: a loop is a closed curve with its starting
point overlapped by its ending point. Because the sample
points within the drifter trajectory are discrete, it is in fact
the overlapping point between the two intersectant trajec-
tory segments (see Appendix A for the details). The total
number of the detected loops is 4360, of which 3532 loops
are anticyclonic and 828 loops are cyclonic. After cluster-
ing the loops, there are in total 2208 eddies identified, of
which 1590 are anticyclonic eddies and 618 are cyclonic ed-
dies (Fig. 4a). The histogram of eddy radii with a bin width
of 5 km is shown in Fig. 5. Note that for the sake of the clarity
of histogram, the eddy radii less than 10 km are not plotted,
because the numbers of these submesoscale anticyclonic and
cyclonic eddies are 1380 and 447, respectively, much bigger
than the numbers of other scale eddies (Fig. 4b). It can be
seen from Fig. 4b that drifters have the ability to character-
ize the submesoscale eddies unresolved by satellite altime-
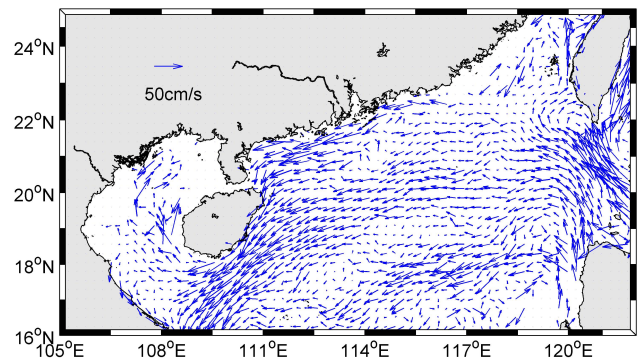ter data. The mean radii of the total eddies, cyclonic eddies

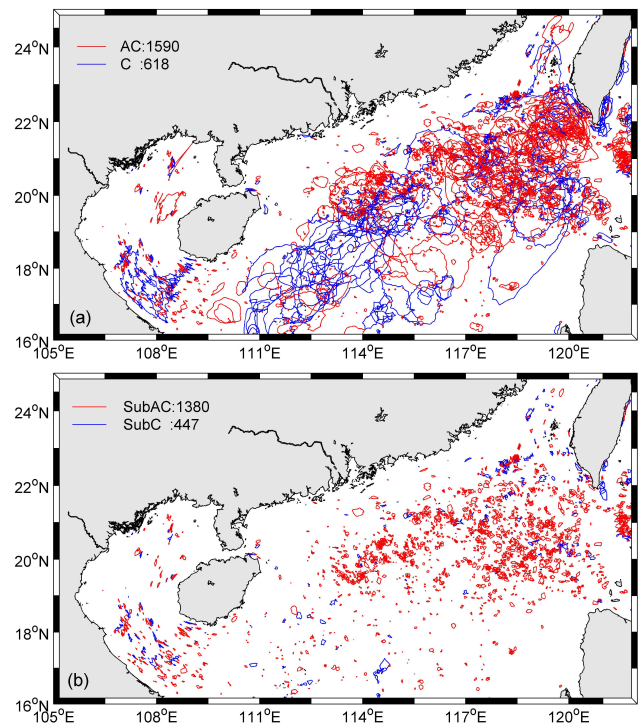**Fig. 3.** Mean flow in the NSCS from averaging all the drifter trajec-
tories.

Fig. 4. (a) Anticyclonic (red) and cyclonic (blue) eddies detected
from drifer trajectories in the NSCS. **(b)** As in **(a)**, but for subme-
soscale anticyclonic (red) and cyclonic (blue) eddies which radii are
less than 10 km.

and anticyclonic eddies are 3.9 km, 3.0 km and 4.9 km, re-
spectively. If the submesoscale eddies (radius < 10 km) are
ignored, the mean radii are 28.7 km, 29.9 km and 27.7 km for
the total, cyclonic and anticyclonic eddies, respectively. It
should be pointed out the eddy sizes calculated from drifters
are often underestimated because the drifter may be con-
trolled by only one part of an eddy (see Fig. 5). If we consider
the drifters are on average statistically evenly distributed
along the eddy radius R, the probability density $p(r, \theta)$ of
finding the drifter at a radius r and direction θ relative to the
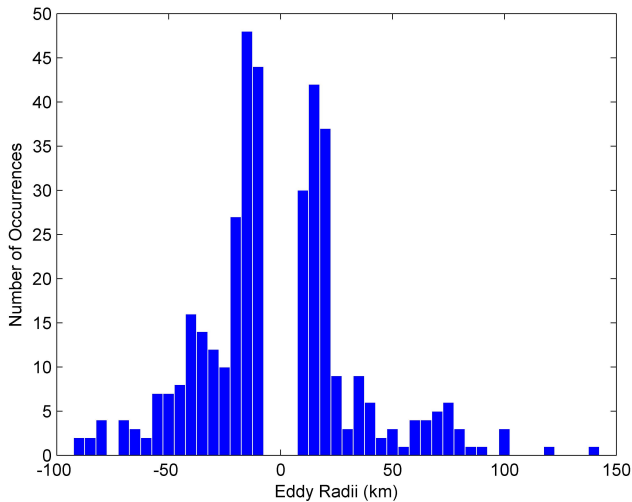eddy center is constant (Chaigneau and Pizarro, 2005):

Fig. 5. Histogram of eddy radii with a bin width of 5 km. Positive radii depict cyclonic eddies, and negative radii depict anticyclonic eddies.

$$p(r,\theta) = \frac{1}{\int\limits_0^R \int\limits_0^{2\pi} r\,dr\,d\theta} = \frac{1}{\pi R^2} \tag{1}$$

The mean distance $\overline{R_1}$, or the expectation

$$E(r) = \int\limits_0^R \int\limits_0^{2\pi} r^2 p(r,\theta)\,dr\,d\theta \tag{2}$$

of the drifter from the eddy center is then given by $\overline{R_1} = 2R/3$. According to this formula, the mean eddy diameter of 7.8 km in the NSCS implies a characteristic eddy diameter of 11.7 km. This order of magnitude is smaller than the Rossby radii (50–90 km) of deformation in the SCS (Chelton et al., 1998).

According to the magnitude of eddy radii, the total eddies can be categorized into three types: large eddies (radius > 60 km), medium eddies (60 km ≥ radius ≥ 10 km) and small (or submesoscale) eddies (radius < 10 km). As for cyclonic (anticyclonic) eddies, the numbers of large, medium and small eddies are 27 (16), 144 (194), 447 (1380), respectively. Wang et al. (2003) examined 8-yr (1993–2000) time series of SSHA, and also found anticyclonic eddies are more than cyclonic eddies in this region. It should be noted that the number of anticyclonic eddies identified from drifters is bigger than that from SSHA. This may be attributed to the different responses of drifters to the surface flow of anticyclonic and cyclonic eddies. Under the right divergent conditions, nutrient-rich cool waters can upwell from deeper waters to act as a seed for the formation of a cold-core (cyclonic) eddy. Likewise, nutrient-poor warmer waters may converge, be downwelled, and a warm-core (anticyclonic) eddy can form. Thus surface flow is divergent for cyclonic

eddies but convergent for anticyclonic eddies. Some may argue that cyclonic eddies in the ocean may be under-sampled by drifters because of the diverging flow, but on the other hand drifters tend to feel the convergent part of the flow associated with anticyclonic eddies. Such argument seems to be supported by both our results and the results of Chaigneau and Pizarro (2005) in the eastern South Pacific, both of which show that more anticyclonic eddies are detected in the drifter trajectories. Thus an open question still remain: how can the biased drifter movements impact on our statistics? Further investigation, including high-resolution numerical simulations, is needed to respond to this question.

3.3 Spatial distribution of eddies

The spatial distribution of cyclonic and anticyclonic eddies from drifters in the NSCS is shown in Fig. 6. We follow Wang et al.'s (2003) geographical delineation of the zones based on the limited knowledge of the eddy generation mechanisms: Zone Z1 (southwest of Taiwan) and Zone Z2 (northwest of Luzon extending west to the 1000 m isobath). In Zone Z1, more anticyclonic eddies are found, most of which are submesoscale anticyclonic eddies (Fig. 6b). Wang et al. (2003) also found the same distribution pattern based on SSHA that anticyclonic eddies with relative small radius and short lifetime are dominant in Zone Z1. In contrast, the number of medium and large cyclonic eddies detected from drifters is a little bigger than that of medium and large anticyclonic eddies in Zone Z2, especially in southeast of Hainan Island (Fig. 6a), while the results of SSHA show that anticyclonic eddies are a little more than cyclonic eddies in Zone Z2. But both indicate the numbers of two kinds of eddies are the same order of magnitude. This small statistical discrepancy may be because Wang et al.'s (2003) criterions used for identifying eddies from SSHA are much strict, such as that the sea level difference between the outermost and the center of an eddy must be greater than 7.5 cm for at least a month. Some cyclonic eddies in Zone Z2 may have not met that criterion, thus they are missed in Wang et al.'s (2003) results.

3.4 Temporal distribution of eddies

The temporal distribution of all the eddies in the NSCS detected from drifters shows that the total number of eddies peaks in May, June, October, November, December and January (Fig. 7a). However, if the submesoscale eddies which radii are less than 10 km are eliminated, it will show another scene: the total number of eddies peaks from November to January of the next year, while declines in March, April, and September (Fig. 7b).

The results of SSHA also indicate that more eddies generate during the winter monsoon (from October to March of the next year) in the NSCS, while less eddies generate during the spring transition period (April and May) and autumn
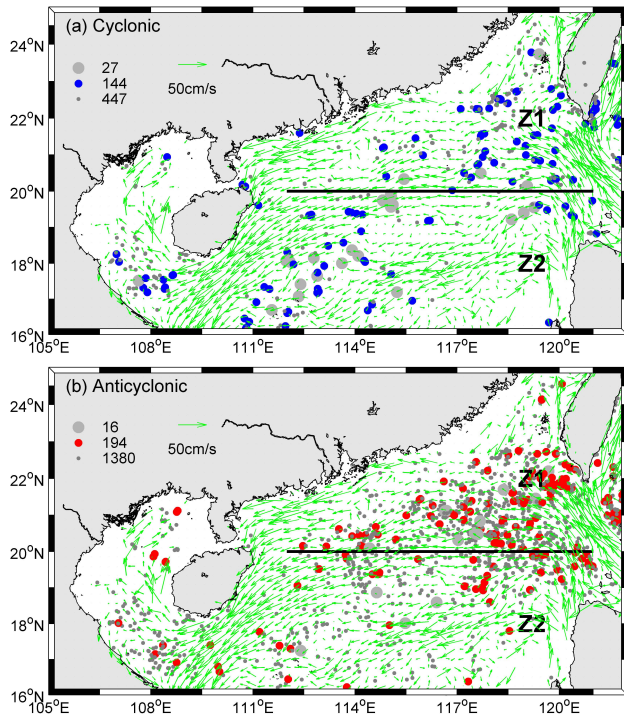
Fig. 6. The distribution of cyclonic **(a)** and anticyclonic **(b)** eddies detected from drifters in the NSCS. Large eddies are shown by the light gray big solid dots, medium eddies by the middle solid dots (blue: cyclonic, red: anticyclonic), and small eddies by the dark gray small solid dots.

Fig. 7. (a) The number of eddies (1979–2010) as a function of the months for cyclonic eddies (blue), anticyclonic eddies (red) and both types of eddies (green). The bars indicate the standard error of eddy number estimates. **(b)** As in **(a)**, but for eddies which radii are bigger than 10 km.

transition period (September) (Wang et al., 2003). This may be related to the eddy generation mechanisms. During the winter monsoon, frontal instability at the Kuroshio intrusion could be one mechanism in shedding eddies in Zone Z1 (Su, 2004). The orographic wind jets associated with the northeast winter monsoon and the gaps in the mountainous island chain along the eastern boundary of SCS can spin up cyclonic and anticyclonic eddies in Zone Z2 (G. Wang et al., 2008).

But why does the total number of eddies including submesoscale eddies peak in May and June? This may be ascribed to the great number of submesoscale eddies which are likely to generate in this period but seldom in the winter monsoon. These results suggest that the submesoscale eddies in the NSCS may not directly related to the upper ocean Ekman response to the wind, but may be related to the process of baroclinic instability (G. H. Wang, personal communication, 2011). The background mechanisms need to be further studied using high-resolution numerical models.

3.5 Tangential velocities of eddies

A linear relationship between the periods and radii of eddies is observed in Fig. 8. There is a significant correlation for both the cyclonic and anticyclonic eddies with orbital period increasing with eddy radius, which shows that cyclonic ed-
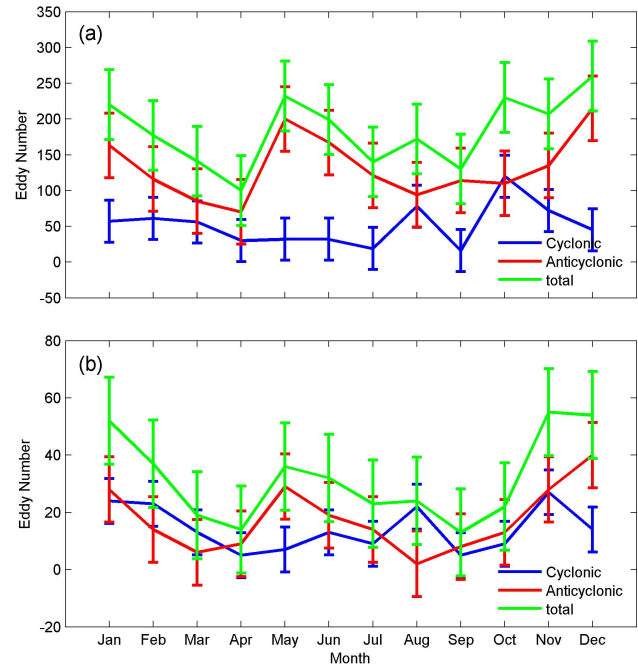
dies tend to rotate more slowly than anticyclonic eddies in the NSCS. This can be validated further in Fig. 9 that shows the scatterplot of eddy radii and tangential velocities for cyclones and anticyclones. We can see that the maximum and mean tangential velocities of anticyclonic eddies are about $40\,\mathrm{cm\,s^{-1}}$ and $25\,\mathrm{cm\,s^{-1}}$, respectively. In contrast, the two values of cyclonic eddies are about $30\,\mathrm{cm\,s^{-1}}$ and $15\,\mathrm{cm\,s^{-1}}$, respectively. If the center of an eddy is in near-solid-body rotation, the period remains constant for increasing radius up to the position of the maximum tangential velocity. Therefore, we can speculate that drifters are entrained into cyclones or anticyclones orbits at distances greater than the maximum tangential velocity.

The reconstructed tangential velocities as a function of eddy radii from all the identified eddies allow us to determine the normalized vorticities of the surface flow (Pingree and Cann, 1992; van Aken, 2002; Chaigneau and Pizarro, 2005):

$$\left|\frac{\xi}{f}\right| = \left|\frac{1}{fr}\right| \left|\frac{\partial(rV_{\mathrm{t}})}{\partial r}\right| \tag{3}$$

where, ξ is the relative vorticity, f is the planetary vorticity, r is the distance to eddy center and V_{t} is the tangential velocity. The normalized vorticity $|\xi/f|$ of the eddies increases when r decreases: at the radius 80 km, $|\xi/f|$ amounts to 0.02 (0.04) for anticyclones (cyclones), the magnitude increasing
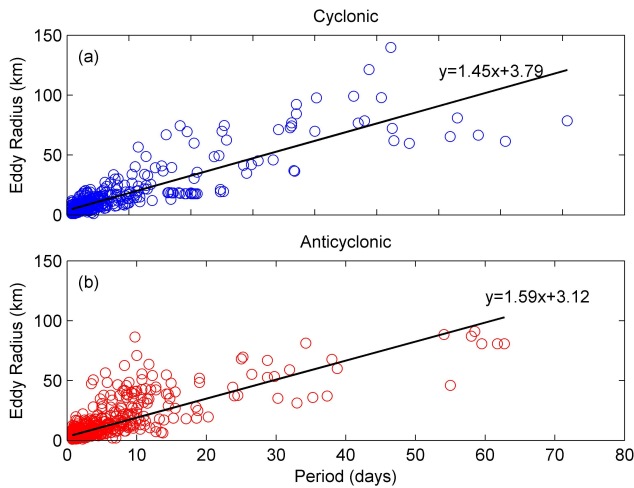
Fig. 8. Relationship between eddy radii and eddy periods for cyclonic eddies **(a)** and anticyclonic eddies **(b)**. The solid lines are the least square fitted lines for cyclonic and anticyclonic eddies.

Fig. 9. Scatterplot of eddy radii and tangential velocities for cyclonic eddies (blue) and anticyclonic eddies (red). The green and yellow lines show the smoothed data for cyclonic and anticyclonic eddies, respectively.

to 0.4 (0.5) for anticyclones (cyclones) within a radius of 10 km (the maximum V_t), and around 0.7 (0.9) near the centers for anticyclones (cyclones). Mesoscale eddies are largely quasi-geostrophic, which are characterized by small Rossby number ($Ro \ll 1$). At the radius of 80 km, the relative vorticity ξ is about 3 % of f, suggesting that mesoscale eddies are in the geostrophic balance. Thus the consideration of the geostrophic relationship to determine the swirl velocity at the eddy edges from altimetry measurements appears to be appropriate for large eddy diameters. Near the center, the vorticity rate ($|\xi/f|$) is about 0.8. Thus a relative vorticity of about 0.8 times the planetary vorticity suggests that eddy cores are ageostrophic. Although the mesoscale eddies may be considered in geostrophic balance, ageostrophic dynamics and centrifugal effects may play an important role for the growth and decay of the mesoscale cores (Chaigneau and Pizarro, 2005). However, processes at submesoscale are distinguished by order one Rossby and Richardson numbers; their dynamics are distinct from those of the quasi-geostrophic mesoscale. They are not described appropriately by the traditional quasi-geostrophic theory that applies to mesoscales (Thomas et al., 2008). It is not fully three-dimensional and nonhydrostatic, either. Many questions remain open in regards with submesoscale eddies because they are notoriously difficult to observe and model.

4 Discussion and conclusions

Based on the in-situ satellite-tracked drifters, eddy characteristics in the NSCS were generally investigated, especially these submesoscale eddies unresolved by SSHA. There are in total 2208 eddies identified, 70 % of which are anticyclonic eddies. The spatial distribution of eddies is regional:
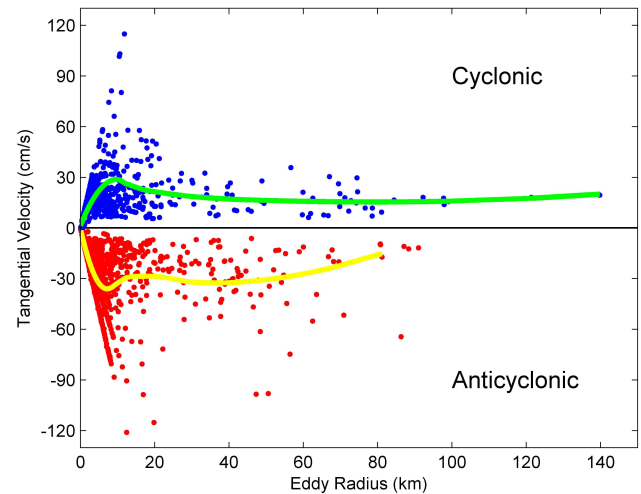
in Zone Z1, the number of anticyclonic eddies dominates the number of cyclonic eddies, most of which are the submesoscale anticyclonic eddies with small radii; whereas, in Zone Z2, the number of large and medium cyclonic eddies is a little greater than the number of anticyclonic eddies. We also notice that if the submesoscale eddies are eliminated, the other eddies in the NSCS will show a 1.2:1 ratio of the number of anticyclones (210) to the number of cyclones (171). It is a very interesting topic to analyze these submesoscale eddies, such as their generation mechanisms and their roles in the water exchange of Luzon Strait. But this is beyond the scope of this research.

The temporal distribution of eddies in the NSCS has a close relation with the Asian monsoon. The total number of large and medium eddies peaks in the winter monsoon, while it tends to decline quickly in the transition periods of monsoon. On the contrary, the submesoscale eddies are likely to generate in the summer monsoon but seldom in the winter monsoon, which may be related to the baroclinic instability. The spatial and temporal patterns have a good agreement with the results of SSHA. This may validate our identification method.

The maximum and mean tangential velocities of anticyclonic (cyclonic) eddies are 40 (30) cm s^{-1} and 25 (15) cm s^{-1}, respectively. This may indicate that anticyclonic eddies tend to rotate more quickly than cyclonic eddies in the NSCS. The normalized vorticities $|\xi/f|$ calculated from all the identified eddies suggest that although the mesoscale eddies may be considered in geostrophic balance, ageostrophic dynamics and centrifugal effects may play an important role for the growth and decay of the mesoscale cores.

In addition, this study may be complementary to the studies based on satellite data in the NSCS. Their combined use is expected to achieve a more complete view of ocean dynamics in the NSCS. This work may also provide useful information for the choice of appropriate spatial resolution of these eddy-resolving models along with developing strategies on future drifter deployments in the NSCS.

Appendix A

Eddy identification method from drifters

Lagrangian drifters have been extensively utilized to track eddies, which are a reliable source of in-situ continuous data comparing with satellite remote sensing data. If the drifter is entrained into an eddy, it can exhibit the looping motion before being ejected. Eddies are thus revealed by clockwise and counterclockwise loops in drifter trajectories. The issue of identifying the coherent eddy structures in the drifter trajectories is then reduced to identifying the looping segments within a trajectory. Manual identification of these loops from drifters has been conducted in many studies (e.g. Shoosmith et al., 2005; Chow et al., 2008). However, this is time-consuming and possibly subject to human error or bias. In order to identify these loops automatically, an identification method based on the geometry of drifter trajectory was developed. This method is different from the geometric method of Boebel et al. (2003), which uses the curvature of drifter trajectory to identify loops. Our method is based on the definition of a loop: a loop is a closed curve with its starting point overlapped by its ending point. Because the sample points within the drifter trajectory are discrete, it is in fact the overlapping point between the two intersectant trajectory segments.

It should be noticed that not all the detected overlapping points correspond to the loops, such as the points C and D in Fig. A1a, which are actually the overlapping points of different loops. These points are called "the false overlapping points", while A and B in Fig. A1a are called "the true overlapping points" corresponding to the loops. To avoid the disturbance of the false overlapping points, we must do the skip searching, not the one by one point searching. Take point A as an example: suppose A is the overlapping point between the two intersectant trajectory segments $(P(i) - P(i+1)$, $P(j) - P(j+1))$, then the subsequent searching should start at point $P(j+1)$ not point $P(i+1)$. This skip can detect the true overlapping points A and B while ignoring the false overlapping points C and D (see Fig. A1a). However, we have noticed that there may exist small internal loops inside a bigger loop (Fig. A1b), which is likely to indicate the smaller eddy disturbance embedded inside the bigger eddy. Thus before the skipping, the internal searching in the range of the detected bigger loop should be made. A smaller loop identified inside a bigger one is shown in Fig. A1b. When the true
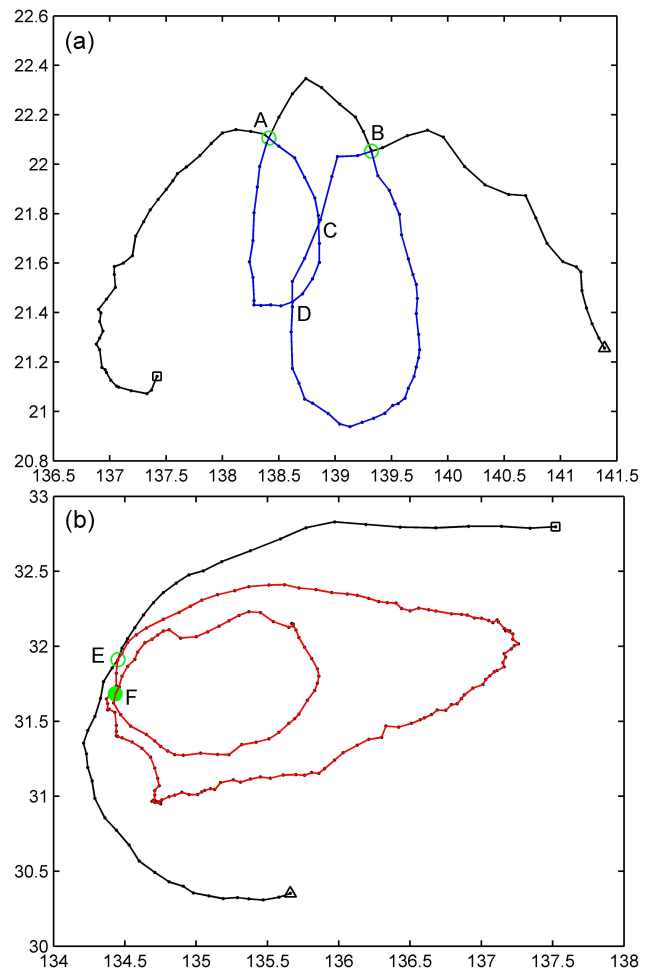

Fig. A1. (a) An example of the loops identified in the drifter trajectory shown with the solid line. The solid points represent the sample points along the drifter trajectory. The starting and ending points of this trajectory are marked with a triangle and a square, respectively. The green empty circles are the true overlapping points marked with A and B, while the false are marked with C and D. **(b)** An example of a bigger loop containing a smaller loop identified. The green empty circle E is the overlapping point of the bigger loop, and the green solid circle F represents the overlapping point of the internal smaller loop. The blue (red) segments are indicated as counter-clockwise (clockwise) loops.

overlapping points are detected, the sample points between the two intersectant lines are the whole loop points. One example that shows the detected loops in a realistic complex drifter trajectory is shown in Fig. A2.

The polarity of a loop is defined according to its rotating direction. In the Northern Hemisphere, when a drifter is caught by a cyclone (anticyclone) eddy, it will make the counter-clockwise (clockwise) loop. The situation is just converse in the Southern Hemisphere. Inspired by Sadarjoen and Post (2000) on a swirling pattern around a central set of points in the streamlines, the winding angle of the loop
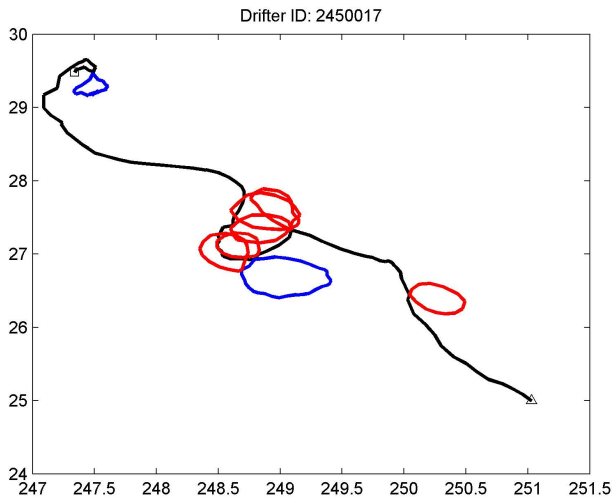
Fig. A2. An example showing the complexity of a realistic drifter trajectory. The blue (red) segments are indicated as counterclockwise (clockwise) loops. The starting and ending points of this trajectory are marked with a triangle and a square, respectively.
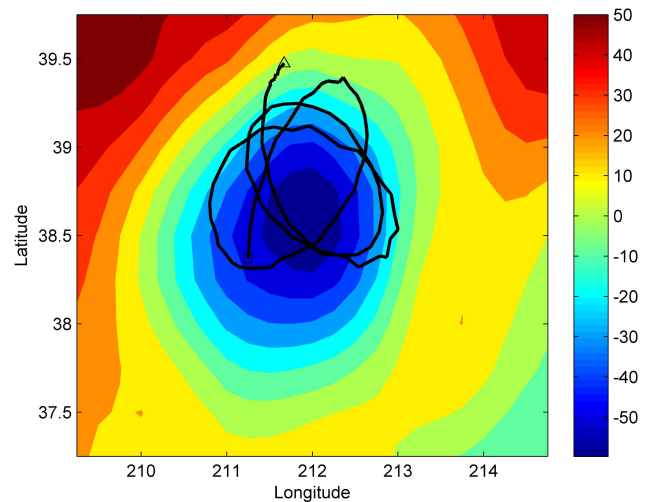

Fig. A3. An example of a drifter (ID: 78922) circumrotating three times when caught by an cyclonic eddy. The black curve shows the drifter trajectory, and the starting and ending points of this trajectory are marked with a triangle and a square, respectively. Colorful filled contours show the SSHA on 10 September 2008, corresponding to the drifter sampling.

trajectory is calculated to determine the polarity of a loop (see more detail in Sadarjoen and Post, 2000). The determined polarities of the detected loops are shown in Figs. A1 and A2.

The loop center can be estimated by geometrically averaging all the sample points in the loop. Here we define the loop radius R by averaging all the distances between the loop points to the loop center. The rotating period T_d of a loop is defined as the time between the starting time and the ending time of the loop segment along the drifter sampling time series. The angle speed L_a can be calculated using the formula $L_a = 2\pi / T_d$, and the tangential speed L_s is $L_s = L_a \times R$.

During the movement of a drifter, if it is caught by an eddy for some time, it is possible the drifter can spin several times following the eddy (see Fig. A3). After extracting all the loops in a drifter trajectory, we can group the loops which are likely to represent the same eddy.

Rather than clustering loops, it is easier to cluster the center points. These center points are clustered as follows: the first point is considered as the first cluster. For each subsequent loop, if its polarity is the same with the first one, then we compute the distance D between the center of the first loop and that of the subsequent loop. Based on the theoretical behavior of eddies embedded in the background flow, a distance criterion was chosen: $D_0 = \overline{U} \times \Delta t$, where $\overline{U}$ is the drifter-derived mean velocity, and Δt is the time interval between two successive loops (defined as $t2 - t1$, where $t1$ is the time at the overlapping point of an loop and $t2$ is the time at the overlapping point of its subsequent loop along a drifter trajectory). Note D_0 is not constant, since $\overline{U}$ and Δt can both vary from site to site. If $D < D_0$, we group the subsequent loop to the first cluster. If $D > D_0$, the subsequent point con-

stitutes a new cluster. After repeating the procedure among all the extracted loops within a drifter trajectory, the loops are combined into a distinct number of groups. Loops of the same group are considered as part of the same eddy. The number of loops representing the same eddy within a drifter trajectory indicates the circumrotating times of the drifter following an eddy.

Edited by: K. J. Heywood

References

Boebel, O., Lutjeharms, J., Schmid, C., Zenk, W., Rossby, T., and Barron, C.: The cape cauldron: a regime of turbulent inter-ocean exchange, Deep-Sea Res. Pt. II, 50, 57–86, 2003.

Chaigneau, A. and Pizarro, O.: Eddy charcteistics in the eastern South Pacific, J. Geophys. Res., 110, C06005, doi:10.1029/2004JC002815, 2005.

Chelton, D. B., Deszoeke, R. A., and Schlax, M. G.: Geographical variability of the first baroclinic Rossby radius of deformation, J. Phys. Oceanogr., 28, 433–460, 1998.

Chow, C.-H., Hu, J.-H., Centurioni, L. R., and Niiler, P. P.: Mesoscale Dongsha cyclonic eddy in the northern South China Sea by drifter and satellite observations, J Geophys. Res., 113, C04018, doi:10.1029/2007JC004542, 2008.

Chu, P. C., Fan, C. W., Lozano, C. J., and Kerling, J. L.: An airborne expendable bathythermograph survey of the South China Sea, May 1995, J. Geophys. Res., 103, 21637–21652, 1998.

Hamilton, P.: Eddy statistics from Lagrangian drifters and hydrography for the northern Gulf of Mexico slope, J. Geophys. Res., 112, C09002, doi:10.1029/2006JC003988, 2007.

Hansen, D. V. and Poulain, P.-M.: Quality control and interpolations of WOCE-TOGA drifter data, J. Atmos. Oceanic. Tech., 13, 900–909, 1996.

Hwang, C. and Chen, S.-A.: Circulations and eddies over the South China Sea derived from TOPEX/Poseidon altimetry, J. Geophys. Res., 105, 23943–23965, doi:10.1029/2000JC900092, 2000.

Jia, Y. L. and Liu, Q. Y.: Eddy shedding from the Kuroshio bend at Luzon Strait, J. Oceanogr., 60, 1063–1069, 2004.

Li, L., Nowlin Jr., W. D., and Su, J. L.: Anticyclonic rings from the Kuroshio in the South China Sea, Deep-Sea Res. Pt. I, 45, 1469–1482, 1998.

Nan, F., He, Z. G., Zhou, H., and Wang, D. X.: Three long-lived anticyclonic eddies in the northern South China Sea, J. Geophys. Res., 116, C05002, doi:10.1029/2010JC006790, 2011.

Pingree, R. D. and Cann, B. Le.: Three anti-cyclonic slope water oceanic eDDIES (SWODDIES) in the Southern Bay of Biscay in 1990, Deep-Sea Res. Pt. I, 39, 1147–1175, 1992.

Qu, T. D.: Upper-layer circulation in the South China Sea, J. Phys. Oceanogr., 30, 1450–1460, 2000.

Qu, T. D., Du, Y., Gan, J. P., and Wang, D. X.: Mean seasonal cycle of isothermal depth in the South China Sea, J. Geophys. Res., 112, C02020, doi:10.1029/2006JC003583, 2007.

Sadarjoen, I. A. and Post, F. H.: Detection, quantification, and tracking of vortices using streamline geometry, Comp. Graph, 24, 333–341, 2000.

Shaw, P. T., Chao, S. Y., and Fu, L.: Sea surface height variations in the South China Sea from satellite altimetry, Oceanol. Acta, 22, 1–17, 1999.

Shoosmith, D. R., Richardson, P. L., Bower, A. S., Rossby, H. T.: Discrete eddies in the northern North Atlantic as observed by looping RAFOS floats, Deep-Sea Res. Pt II, 52, 637–650, 2005.

Su, J. L.: Overview of the South China Sea circulation and its influence on the coastal physical oceanography outside the Pearl River Estuary, Cont. Shelf. Res., 24, 1745–1760, 2004.

Su, J. L., Xu, J. P., Cai, S. Q., and Wang, O.: Gyres and eddies in the South China Sea, onset and evolution of the South China Sea monsoon and its interaction with the ocean, edited by: Yihui, D. and Chongyin, L., China Meteorological Press, Beijing, China, 272–279, 1999 (in Chinese).

Swenson, M. S. and Niiler, P. P.: Statistical analysis of the surface circulation of the California Current, J. Geophys. Res., 101, 22631–22645, 1996.

Thomas, L. N., Tandon, A., and Mahadevan, A.: Submesoscale processes and dynamics. Eddy Resolving Ocean Modeling, edited by: Hecht, M. W. and Hasumi, H., Amer. Geophys. Union, 17–38, 2008.

van Aken, H. M.: Surface currents in the Bay of Biscay as observed with drifters between 1995 and 1999, Deep-Sea Res. Pt. I, 49, 1071–1086, 2002.

Wang, D. X., Xu, H. Z., Lin, J., and Hu, J. Y.: Anticyclonic eddies in the northeastern South China Sea during winter 2003/2004, J. Oceanogr., 64, 925–935, 2008.

Wang, G. H., Su, J. L., and Chu, P. C.: Mesoscale eddies in the South China Sea observed with altimeter data, Geophys. Res. Lett., 30, 2121, doi:10.1029/2003GL018532, 2003.

Wang, G. H., Su, J. L., and Li, R. F.: Mesoscale eddies in the South China Sea and their impact on temperature profiles, Acta Oceanol. Sinica, 24, 39–45, 2005.

Wang, G. H., Chen, D. K., and Su, J. L.: Generation and life cycle of the dipole in the South China Sea summer circulation, J. Geophys. Res., 111, C06002, doi:10.1029/2005JC003314, 2006.

Wang, G. H., Chen, D. K., and Su, J. L.: Winter eddy genesis in the eastern South China Sea due to orographic wind jets, J. Phys. Oceanogr., 38, 726–732, 2008.

Yuan, D. L., Han, W. Q., and Hu, D. X.: Surface Kuroshio path in the Luzon Strait area derived from satellite remote sensing data, J. Geophys. Res., 111, C11007, doi:10.1029/2005JC003412, 2006.

Yuan, D. L., Han, W. Q., and Hu, D. X.: Anti-cyclonic eddies northwest of Luzon in summer-fall observed by satellite altimeters, Geophys. Res. Lett., 34, L13610, doi:10.1029/2007GL029401, 2007.